Inorganic Chemistry

Article

pubs.acs.org/IC

Carbohydrate-Appended Tumor Targeting Iron(III) Complexes Showing Photocytotoxicity in Red Light

Uttara Basu,[†] Imran Khan,[‡] Akhtar Hussain,[†] Bappaditya Gole,[†] Paturu Kondaiah,*[,‡] and Akhil R. Chakravarty*[,†]

[†]Department of Inorganic and Physical Chemistry, Indian Institute of Science, Bangalore 560012, Karnataka, India

[‡]Department of Molecular Reproduction, Development and Genetics, Indian Institute of Science, Bangalore 560012, Karnataka, India

Supporting Information

ABSTRACT: Glucose-appended photocytotoxic iron(III) complexes of a tridentate Schiff base phenolate ligand [Fe(bpyag)(L)](NO$_3$) (**1**−**3**), where bpyag is *N*,*N*-bis(2-pyridylmethyl)-2-aminoethyl-β-D-glucopyranoside and H$_2$L is 3-(2-hydroxyphenylimino)-1-phenylbutan-1-one (H$_2$phap) in **1**, 3-(2-hydroxyphenylimino)-9-anthrylbutan-1-one (H$_2$anap) in **2**, and 3-(2-hydroxyphenylimino)-1-pyrenylbutan-1-one (H$_2$pyap) in **3**, were synthesized and characterized. The complex [Fe(dpma)(anap)](NO$_3$) (**4**), having bis-(2-pyridylmethyl)benzylamine (dpma), in which the glucose moiety of bpyag is substituted by a phenyl group, was used as a control, and the complex [Fe(dpma)(anap)](PF$_6$) (**4a**) was structurally characterized by X-ray crystallography. The structure shows a FeN$_4$O$_2$ core in a distorted octahedral geometry. The high-spin iron(III) complexes with magnetic moment value of ∼5.9 μ_B showed a low-energy phenolate-to-Fe(III) charge-transfer (CT) absorption band as a shoulder near 500 nm with a tail extending to 700 nm and an irreversible Fe(III)−Fe(II) redox couple near −0.6 V versus saturated calomel electrode. The complexes are avid binders to calf thymus DNA and showed photocleavage of supercoiled pUC19 DNA in red (647 nm) and green (532 nm) light. Complexes **2** and **3** displayed significant photocytotoxicity in red light, with an IC$_{50}$ value of ∼20 μM in HeLa and HaCaT cells, and no significant toxicity in dark. The cell death is via an apoptotic pathway, by generation of reactive oxygen species. Preferential internalization of the carbohydrate-appended complexes **2** and **3** was evidenced in HeLa cells as compared to the control complex **4**. A 5-fold increase in the cellular uptake was observed for the active complexes in HeLa cells. The photophysical properties of the complexes are rationalized from the density functional theory calculations.

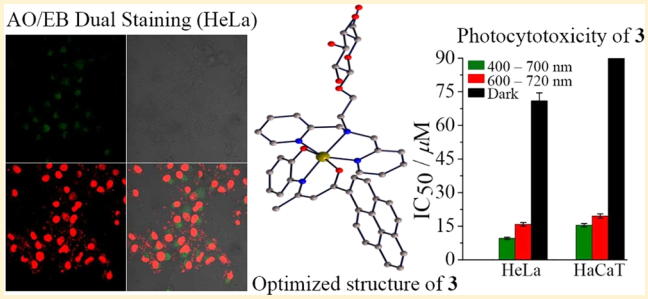

INTRODUCTION

Photodynamic therapy (PDT) has emerged as a noninvasive treatment modality of cancer.[1,2] The therapeutic efficacy of conventional PDT is based on the generation of singlet oxygen as the reactive oxygen species (ROS) on light activation of the photosensitizer (PS). The PS in its triplet excited state transfers its energy to molecular oxygen to form singlet oxygen ($^1O_2$) via type-II process. Alternatively, it might undergo electron transfer reactions to form hydroxyl ($HO^•$) and/or superoxide ($O_2^{•-}$) radicals in a photoredox pathway.[3] The cytotoxic ROS causes oxidative cell damage or death.[4] One important aspect in designing PDT agent is to have selective accumulation of the PS in the cancerous cells leaving the normal and healthy cells unaffected. There should be moderately enhanced accumulation of the PS in the tumor tissues and additional level of selectivity could be achieved by irradiating the tumor cells leaving unexposed healthy cells unaffected. The targeting efficacy of a PDT agent could be improved by ensuring its selective accumulation inside the tumor cells. This can be achieved by designing complexes having ligands conjugated to sugar, peptides, aptamers, etc. binding to specific receptors that overexpress on the cancer cells.[5]

The higher rate of glucose metabolism is a general characteristic of tumor cells.[6,7] The overexpression of glucose transporter GLUT-1 is well documented for a large variety of tumors and tagging a sugar moiety to the ligand could ensure higher uptake of the metal complex in tumor cells while increasing its aqueous solubility.[6−9] Glycoconjugation is reported to be an effective way of increasing the interactions of the conjugates with lectin type receptors that are overexpressed in certain malignant cells.[10−14] Sugar-dependent photocytotoxicity and cellular uptake using glycoconjugated porphyrins and chlorins are reported.[15,16] Recently, functionalization with mannose of photosensitizable nanoparticles is shown to give enhanced PDT effect due to an active endocytosis mediated by a membrane receptor.[17,18]

The conventional PDT agents based on macrocyclic organic dyes show prolonged skin sensitivity, hepatotoxicity and the necessity to have a high quantum yield of generation of singlet oxygen.[2] Metal complexes with their tunable coordination environment and varied spectral and redox properties are

Received: November 11, 2013
Published: January 27, 2014

   dx.doi.org/10.1021/ic4028173 | *Inorg. Chem.* 2014, 53, 2152−2162

potent alternatives to these organic dyes.[19−28] Besides, the metal complexes can generate different types of ROS using the redox property of the transition metal. We have earlier shown that suitably designed 3d metal complexes are potent photocytotoxic agents in PDT.[29−34] An iron(III) complex is shown to be PDT active in red light.[34] In our continued efforts to develop new iron(III)-based PDT agents, we have now designed and studied the photocytotoxic effect of carbohydrate-appended iron(III) complexes in two different cell lines using red light. Herein, we present the iron(III) complexes of a tridentate Schiff base phenolate ligand [Fe(bpyag)(L)](NO_3) (**1**−**3**), where bpyag is *N*,*N*-bis(2-pyridylmethyl)-2-aminoethyl-*β*-D-glucopyranoside (bpyag) and H_2L is 3-(2-hydroxyphenylimino)-1-phenylbutan-1-one (H_2phap) in **1**, 3-(2-hydroxyphenylimino)-9-anthrylbutan-1-one (H_2anap) in **2** and 3-(2-hydroxyphenylimino)-1-pyrenylbutan-1-one (H_2pyap) in **3** (Chart 1). [Fe(dpma)(anap)](NO_3) (**4**) having bis-(2-pyridylmethyl)benzylamine (dpma) in which the glucose moiety of bpyag is substituted by a phenyl group was used as a control and [Fe(dpma)(anap)](PF_6) (**4a**) was structurally characterized by X-ray crystallography. The coordination environment of the metal is modified from the previously reported iron(III)-catechol system by blocking the sixth coordination site of iron(III). This modification ensures better stability of the complexes under physiological conditions by protecting it from possible attack by transferrin at the labile coordination site. Transferrin which has an innate affinity for iron(III) is expected to leach the metal out from the complex by attacking through any vacant or labile site. The use of two different tridentate ligands in the present ternary structure is expected to prevent leaching of iron from the complex. The anthracenyl or pyrenyl pendant group as planar aromatic moiety is expected to increase the DNA binding strengths of the complexes. Complex **1** is used as a control. Similarly, complex **4** having the carbohydrate group replaced with a phenyl group is used to ascertain the role of the sugar moiety in the cellular uptake. The photocytotoxic properties of the complexes in visible light (400−700 nm) and red light (600−720 nm), and their differential uptake properties in HeLa cells are studied. The sugar appended complexes show significantly higher cellular uptake than the control species.

Chart 1. Schematic Drawing of the Complexes 1−4

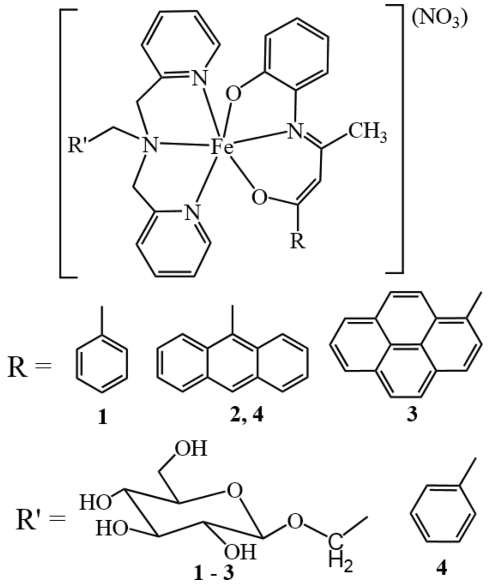

EXPERIMENTAL SECTION

Materials and Methods. All reagents and chemicals were purchased from commercial sources (s.d. Fine Chemicals, India; Sigma-Aldrich, U.S.A.) and used as such without further purifications. Solvents were purified by standard procedures.[35] Supercoiled (SC) pUC19 DNA (cesium chloride purified) was purchased from Bangalore Genie. Tris-(hydroxymethyl)aminomethane-HCl (Tris-HCl) buffer solution was prepared using deionized and sonicated triple distilled water. Calf thymus DNA (ct-DNA), catalase, superoxide dismutase (SOD), 2,2,6,6-tetramethyl-4-piperidone (TEMP), 1,4-diazabicyclo[2.2.2]octane (DABCO), 2′,7′-dichlorofluoresceindiacetate (DCFDA), Hoechst 33258, ethidium bromide (EB), 3-(4,5-dimethylthiazol-2-yl)-2,5-diphenyltetrazolium bromide (MTT), propidium iodide (PI), acridine orange (AO), Dulbecco's modified eagle medium (DMEM), Dulbecco's phosphate buffered saline (DPBS), and fetal bovine serum (FBS) were purchased from Sigma. The carbohydrate-appended dipicolylamine ligand was synthesized by a reported procedure.[36] Ligand 3-(2-hydroxyphenylimino)-1-phenylbutan-1-one (H_2phap) was synthesized by refluxing a mixture of benzoylacetone and 2-aminophenol in methanol for 3 h.[37]

The elemental analysis was done using a Thermo Finnigan Flash EA 1112 CHNS analyzer. The infrared and electronic spectra were recorded using Bruker Alpha and PerkinElmer Spectrum 650 spectrophotometers, respectively. Emission spectral measurements were carried out with a PerkinElmer LS 55 spectrophotometer. Molar conductivity measurements were done using a Control Dynamics (India) conductivity meter. Cyclic voltammetric measurements were made at 25 °C on a EG&G PAR Model 253 VersaStat potentiostat/galvanostat with an electrochemical analysis software 270 using a three electrode setup comprising a glassy carbon working, a platinum wire auxiliary and a saturated calomel reference (SCE) electrode. Tetrabutylammonium perchlorate (TBAP, 0.1 M) was used as a supporting electrolyte. The electrochemical data were uncorrected for junction potentials. Electrospray ionization mass spectral measurements were done using Esquire 3000 plus ESI (Bruker Daltonics) and Q-TOF Mass spectrometers. ^{1}H NMR spectral measurements were made using a Bruker 400 MHz NMR spectrometer. Flow cytometry (FACS) measurements were done using Calibur (Becton Dickinson (BD) cell analyzer) at FL1 channel. Magnetic susceptibility measurement of the complex at 300 K was done with solid sample using MPMS SQUID VSM (Quantum Design, USA). Inductively coupled plasma optical emission spectral measurements were carried out using Perkin-Elmer ICP-OES (Model Optima 2000 DV). Viscometric measurements were performed with a Schott AVS 310 automated viscometer. Imaging studies were performed with a Zeiss LSM 510 apochromat confocal laser scanning microscope (AO/EB dual staining) or Olympus IX 81 fluorescence microscope (PI staining).

Synthesis. The ligands 3-(2-hydroxyphenylimino)-9-anthrylbutan-1-one (H_2anap) and 3-(2-hydroxyphenylimino)-1-pyrenylbutan-1-one (H_2pyap) were synthesized by a three-step general procedure in which anthracene or pyrene was first acetylated with acetyl chloride. The acetylated product was refluxed with ethyl acetate in presence of sodium sand to obtain 9-anthroylacetone or pyrenoylacetone by Claisen condensation reaction. Finally, 9-anthroylacetone or pyrenoylacetone was refluxed with 2-aminophenol in methanol for 8−10 h to obtain yellow crystals of the product from the filtrate upon standing at room temperature.

3-(2-Hydroxyphenylimino)-9-anthrylbutan-1-one (H_2anap).[38] A solution of anthracene (5 g, 28 mmol) and acetyl chloride (12 mL, 168.3 mmol) in dry CH_2Cl_2 (100 mL) was cooled in an ice-salt bath. $AlCl_3$ (7.48 g, 56.1 mmol) was added with vigorous stirring maintaining the temperature below 0 °C. The solution was stirred for 1 h at the bath temperature and then gradually warmed to 10 °C. The brick red solution was poured into a mixture of ice and concentrated HCl. The product was extracted with CH_2Cl_2, washed with water (3 × 50 mL) and dried over anhydrous sodium sulfate.

dx.doi.org/10.1021/ic4028173 | Inorg. Chem. 2014, 53, 2152−2162

Removal of the solvent gave shiny red oil that solidified upon standing. The crude product was dissolved in hot ethanol (~50 mL) and heated to reflux for 30 min and cooled rapidly to room temperature. The solution was filtered and heated again. Slow cooling gave orange-brown crystals of the acetylated product that was filtered and dried in vacuum (4.4 g, 73%). A solution of 9-acetylanthracene (11 g) in ethyl acetate (24 mL), dry ether (70 mL) was quickly added to sodium sand (2.2 g). After the vigorous reaction subsided, the mixture was refluxed for 4 h, cooled and poured into water (70 mL). The aqueous layer was acidified with acetic acid and the crude 9-anthroylacetone was recrystallized twice from EtOH by filtering over activated charcoal. 9-Anthroylacetone (2.62 g, 10 mmol) was dissolved in methanol (50 mL) by warming. To it was added 2-aminophenol (1.09 g, 10 mmol). The orange mixture was refluxed for 8 h. A yellow precipitate thus formed was filtered and air-dried. The second crop of product in the form of yellow-orange crystals was obtained from the filtrate upon standing for a couple of days (Yield: ~80%). ^{1}H NMR ($CDCl_3$, 400 MHz) δ (ppm): 8.470 (s, 1H), 8.216 (t, J = 9.6 Hz, 2H), 8.022 (t, J = 9.6 Hz, 2H), 7.484 (m, 4H), 7.121 (m, 1H), 6.926 (m, 1H), 6.623 (m, 1H), 5.704 (s, 1H), 2.033 (s, 3H) (s, singlet; t, triplet; m, multiplet; J, coupling constant).

3-(2-Hydroxyphenylimino)-1-pyrenylbutan-1-one (H_2pyap).[39] $AlCl_3$ (10 g) was suspended in dry CH_2Cl_2 (100 mL) and cooled below 0 °C in an ice-salt bath. Acetyl chloride (5.15 g) was gradually added and stirred for 15 min. Pyrene (12.6 g) was added in portions, and the dark-red reaction mixture was stirred at room temperature for 18 h under N_2 atmosphere. Ice cold concentrated HCl (~5 mL) was added. The reaction mixture was stirred for 15 min and poured over ice. The product was extracted with CH_2Cl_2, washed with water (3 × 50 mL), and dried over anhydrous sulfate. The solvent was evaporated to afford a yellow oil, which solidified upon standing. The product was recrystallized from methanol to get bright yellow crystals (Yield: ~80%). ^{1}H NMR ($CDCl_3$, 400 MHz): δ 9.031 (d, J = 8.2 Hz, 1H), 8.342 (d, J = 8.0 Hz, 1H), 8.209 (m, 3H), 8.123 (m, 2H), 8.026 (m, 2H), 2.885 (s, 3H) (d, doublet).

A solution was formed of acetylpyrene (3 g) in ethylacetate (8 mL), and dry ether (25 mL) was quickly added to sodium sand (0.65 g). After the vigorous reaction subsided, the mixture was refluxed for 24 h. Water was added slowly, and the aqueous layer was acidified with acetic acid when a yellow precipitate formed. It was filtered and air-dried. The crude product was purified by column chromatography, eluting with 2% CH_2Cl_2–MeOH. The solvent was evaporated to get the pure product pyrenoylacetone as a yellow-orange powder (yield: ~70%). ^{1}H NMR ($CDCl_3$, 400 MHz): δ 8.782 (d, 9.2 Hz, 1H), 8.262–7.994 (m, 8H), 6.207 (s, 1H), 2.276 (s, 3H). Pyrenoylacetone (2.86 g, 10 mmol) was dissolved in methanol (50 mL) by warming. To it was added 2-aminophenol (1.09 g, 10 mmol). The orange mixture was refluxed for 10 h. The yellow precipitate formed was filtered and air-dried. A second crop of the product was obtained as yellow-orange crystals from the filtrate upon standing for 2 d (yield: ~80%). ^{1}H NMR ($CDCl_3$, 400 MHz): δ 8.781 (d, 9.2 Hz, 1H), 8.266–8.019 (m, 9H), 7.230–6.912 (m, 3H), 5.947 (s, 1H), 2.061 (s, 1H).

*Syntheses of the complexes [Fe(bpyag)(L)](NO$_3$) (L = phap, **1**; anap, **2**; pyap, **3**) and [Fe(dpma)(anap)](NO$_3$) (**4**).* The complexes were prepared by a general procedure in which $Fe(NO_3)_3{\cdot}9H_2O$ (0.404 g, 1 mmol) in methanol (5 mL) was reacted with the carbohydrate-appended dipicolylamine (0.405 g, 1 mmol, for **1**–**3**) or phenyl dipicolylamine (0.289 g, 1 mmol, for **4**) in methanol (6 mL) and stirred at room temperature for 30 min and filtered. The methanol solution of the ligand, namely, H_2phap or H_2anap or H_2pyap (1 mmol), was subsequently added to the filtrate after treating with 2 equiv of triethylamine. The solution was further stirred for another 2 h at 25 °C and filtered. The filtrate was evaporated to obtain the complexes as dark-red solid.

*[Fe(bpyag)(phap)](NO$_3$) (**1**).* Yield: ~78% (0.6 g). Anal. Calcd for $C_{36}H_{40}FeN_5O_{11}$: C, 55.82; H, 5.21; N, 9.04. Found: C, 55.71; H, 5.29; N, 9.24%. ESI-MS in MeCN (m/z): 712.22 $[M\text{-}NO_3^-]^+$. Molar Conductance in dimethylformamide (DMF) (Λ_M): 69 S m^2 M^{-1}. Fourier transform infrared (FT-IR) spectroscopy: 3320 br (O–H), 2930 w, 2600 w, 2490 w, 1590 w, 1440 m, 1370 m (NO_3^-), 1290 w, 1030 vs, 760 w, 570 m (vs, very strong; m, medium; w, weak; br, broad). Ultraviolet–visible (UV–vis) spectroscopy in 5% DMF–Tris-HCl buffer, pH 7.2 [λ_{max} (nm) (ε/ M^{-1} cm^{-1})]: 560 (720), 395 (3240), 330 (3500). μ_{eff} (298 K) = 5.83 μ_B.

*[Fe(bpyag)(anap)](NO$_3$) (**2**).* Yield: ~74% (0.65 g). Anal. Calcd for $C_{44}H_{44}FeN_5O_{11}$: C, 60.42; H, 5.07; N, 8.01. Found: C, 60.33; H, 5.16; N, 8.12%. ESI-MS in MeCN (m/z): 812.38 $[M\text{-}NO_3^-]^+$. Molar conductance in DMF (Λ_M): 72 S m^2 M^{-1}. FT-IR: 3350 br (O–H), 2990 w, 2700 w, 1640 m, 1460 m, 1370 m (NO_3^-), 1030 vs, 740 w, 550 m. UV–vis in 5% DMF–Tris-HCl buffer, pH 7.2 [λ_{max} (nm) (ε/ M^{-1} cm^{-1})]: 505sh (1240), 392 (6790), 373 (6430), 355 (5390) (sh, shoulder). μ_{eff} (298 K) = 5.85 μ_B.

*[Fe(bpyag)(pyap)](NO$_3$) (**3**).* Yield: ~70% (0.63 g). Anal. Calcd for $C_{46}H_{44}FeN_5O_{11}$: C, 61.48; H, 4.93; N, 7.79. Found: C, 61.53; H, 4.75; N, 7.69%. ESI-MS in MeCN (m/z): 836.25 $[M\text{-}NO_3^-]^+$. Molar Conductance in DMF (Λ_M): 71 S m^2 M^{-1}. FT-IR: 3360 br (O–H), 2990 w, 2700 w, 2500 w, 1640 m, 1470 m, 1380 m (NO_3^-), 1030 vs, 740w, 570 m. UV–vis in 5% DMF–Tris-HCl buffer, pH = 7.2 [λ_{max} (nm) (ε/ M^{-1} cm^{-1})]: 490 sh (1400), 393(12920), 372 (14070), 352 (10770), 334 (7690). μ_{eff} (298 K): 5.83 μ_B.

*[Fe(dpma)(anap)](NO$_3$) (**4**).* Yield: ~83% (0.63 g). Anal. Calcd for $C_{43}H_{36}FeN_5O_5$: C, 68.08; H, 4.78; N, 9.23. Found: C, 68.15; H, 4.71; N, 9.27%. ESI-MS in MeCN (m/z): 696.33 $[M\text{-}NO_3^-]^+$. Molar Conductance in DMF (Λ_M): 70 S m^2 M^{-1}. FT-IR: 3210 w, 3000 w, 1600 w, 1450 w, 1360 m (NO_3^-), 1030 w, 830 vs, 540 s (s, strong). UV–vis in 5% DMF–Tris-HCl buffer, pH = 7.2 [λ_{max} (nm) (ε/ M^{-1} cm^{-1})]: 434 sh (3890), 389 (5860), 369 (5050), 350 (4010). μ_{eff} (298 K): 5.86 μ_B.

X-ray Crystallographic Procedures. The crystal structure of complex **4** as its PF_6 salt (**4a**) was obtained by single-crystal X-ray diffraction technique. Crystals were obtained from the slow evaporation of a methanol–acetonitrile (1:1 v/v) solution of the complex. Crystal mounting was done on glass fiber with epoxy cement. All geometric and intensity data were collected at room temperature using an automated Bruker SMART APEX CCD diffractometer equipped with a fine focus 1.75 kW sealed tube Mo K_α X-ray source (λ = 0.71073 Å) with increasing ω (width of 0.3° per frame) at a scan speed of 5 and 15 s per frame. Intensity data, collected using ω-2θ scan mode, were corrected for Lorentz–polarization effects and for absorption.[40] Structure was solved by the combination of Patterson and Fourier techniques and refined by full-matrix least-squares method using SHELX system of programs.[41] The hydrogen atoms belonging to the complex were in their calculated positions and refined using a riding model. All non-hydrogen atoms were refined anisotropically. The molecular view was obtained by ORTEP.[42] Selected crystallographic data are given in Table S1 (Supporting Information). The CCDC number is 958281.

Cytotoxicity. The photocytotoxicity of the complexes was studied using MTT assay, which is based on the ability of mitochondrial dehydrogenases of viable cells to cleave the tetrazolium rings of MTT, forming dark-purple membrane-impermeable crystals of formazan that could be quantified from spectral measurement in DMSO.[43] Approximately 8000 cells of human cervical cancer (HeLa) cells or keratinocyte (HaCaT) cells were plated separately in a 96 wells culture plate in Dulbecco's Modified Eagle Medium (DMEM) containing 10% FBS. After 24 h of incubation at 37 °C in 5% CO_2 atm, various concentrations of the complexes dissolved in 1% DMSO were added to the cells, and incubation was continued for 2 and 4 h in dark. The media was subsequently replaced with DPBS and irradiated with a broad band visible light (400–700 nm, 10 J cm^{-2}), using a Luzchem Photoreactor (Model LZC-1, Ontario, Canada) fitted with Sylvania make 8 fluorescent white tubes or a red light of 600–720 nm (150 J cm^{-2}), using Waldmann PDT 1200 L. After photoexposure, DPBS was removed and replaced with DMEM–FBS, and incubation was continued for a further period of 20 h in dark. After the incubation period, 5 mg mL^{-1} of MTT (20 μL) was added to each well, and incubation continued for an additional 3 h. The culture medium was finally discarded, and 200 μL of DMSO was added to dissolve the formazan crystals; the absorbance of the culture medium at 540 nm was measured using a Molecular Devices Spectra Max M5 plate reader.

dx.doi.org/10.1021/ic4028173 | Inorg. Chem. 2014, 53, 2152–2162

Cytotoxicities of the complexes were measured as the percentage ratio of the absorbance of the treated cells to the untreated controls. The IC_{50} values were determined by nonlinear regression analysis (GraphPad Prism 5).

Quantification of Cellular Iron by ICPOES. For cellular uptake studies by inductively coupled optical emission spectroscopy (ICPOES), HeLa or HaCaT cells were grown in 6 well tissue culture plates in DMEM supplemented with 10% FBS to 80% confluency. The complexes **1**−**4** were dissolved in DMSO and added to the cells to give a final complex concentration of 10 μM (final concentration of DMSO 1% v/v). They were incubated for 2 and 4 h at 37 °C in a CO_2 incubator. The culture medium was discarded, and the cells were washed thrice with ice-cold DPBS. The cells were harvested, taken up in DPBS, and centrifuged at 3000 rpm for 15 min. After discarding the buffer, the cell pellets were dissolved in 70% nitric acid at 65 °C for 2 h. The samples were diluted further to a final concentration of 5% nitric acid with double-distilled water containing 0.1% Triton X100. The iron content inside the cells was estimated using the spectrometer previously calibrated with standard ferric nitrate solutions. The protein content inside the cells was estimated by Bradford assay after lysing the cells with 1 N NaOH solution. The quantity of iron was expressed as ng/mg of protein.

DNA Fragmentation Analysis. The analysis was carried out to ascertain the apoptotic mechanism induced by the complexes **2** and **3** for cell death. Briefly, 0.3×10^6 cells were taken in 6 well plates, grown for 24 h and later treated with the complexes (10 μM) for 4 h in dark. Light was exposed to one of the dishes for 1 h, and again the cells were left to grow for 4 h, along with their dark control. After 4 h, cells were trypsinized, washed with DPBS, and resuspended in 0.4 mL of lysis buffer (10 mM Tris-HCl, pH = 8.0, 20 mM ethylenediaminetetraacetate (EDTA), 0.2% triton-X 100), with an incubation of 20 min in ice. Lysed cells were centrifuged for 20 min at 13 000 rpm, and their supernatants, having soluble chromosomal DNAs, including both high molecular weight DNA and nucleosomal DNA fragments, were collected. Phenol/chloroform treatment was performed to remove the protein present. The supernatant was precipitated with 1/10 volume of 3 M sodium acetate (pH = 5.8) and 2 volumes of ethanol at −20 °C for overnight. DNA pellet was washed with 70% alcohol and resuspended in TE containing RNase (1X Tris-EDTA with 100 μg mL^{-1} RNase). DNA samples were placed into the well of 1.5% agarose gel. The agarose gels were run at 70 V for approximately 2 h before they were photographed under UV light.

DCFDA Assay for ROS Generation. The DCFDA was used to detect the generation of cellular ROS.[44] Cell-permeable DCFDA could be oxidized by cellular ROS to generate a fluorescent 2′,7′-dichlorofluorescein (DCF) with an emission maxima at 525 nm.[45] The percentage population of cells generating ROS was determined by flow cytometry analysis in which HeLa or HaCaT cells were incubated with the complexes **2** and **3** (10 μM) for 4 h followed by irradiation with visible light (400−700 nm) for 30 min in serum-free conditions. The cells were harvested by trypsinization, and a single-cell suspension of 1×10^6 cells mL^{-1} was made. The cells were then treated with 1 μM DCFDA solution in DMSO in dark for 15−20 min at 25 °C. The distribution of DCFDA-stained HeLa cells was determined by flow cytometry in the FL-1 channel.

Fluorescence Activated Cell Sorting (FACS) Analysis. To investigate the effect of complexes **2**−**4** on the cell cycle, 3×10^6 HeLa cells were plated per well of a 6-well tissue culture plate in DMEM containing 10% FBS. After 24 h of incubation at 37 °C in a CO_2 incubator, DMSO solutions of complexes **2**−**4** (10 μM) were added to the cells, and incubation was continued in dark for 2 h. The medium was subsequently replaced with DPBS, and irradiation was done with visible light (400−700 nm) using a Luzchem Photoreactor. After irradiation, DPBS was removed and replaced with DMEM containing 10% FBS, and incubation was continued in the dark for a further period of 12 h. Cells were then trypsinized and collected into 1.5 mL centrifuge tubes. The cells were washed once with DPBS (pH = 7.4) and fixed by adding 800 μL of chilled 70% methanol dropwise with constant and gentle vortexing to prevent any cell aggregation. The cell suspensions were incubated at −20 °C for 6 h. The fixed cells were then washed twice with 1.0 mL of DPBS by centrifuging at 4000 rpm at 4 °C for 5 min. The supernatants were gently discarded, and the cell pellets were suspended in 200 μL of DPBS containing 10 μg mL^{-1} DNase-free RNase at 37 °C for 12 h. After digestion of cellular RNA, a 20 μL volume of 1.0 mg mL^{-1} propidium iodide solution was added to both the mixtures, which were incubated at 25 °C in the dark for another 20 min. Flow cytometric analysis was performed using a FACS Calibur [Becton Dickinson (BD) cell analyzer] at FL2 channel (595 nm), and the distribution of cells in various cell-cycle phases was determined from the histogram generated by Cell Quest Pro software (BD Biosciences). Data analysis for the percentage of cells in each cell-cycle phase was performed by using WinMDI version 2.8.

Ethidium Bromide/Acridine Orange Dual Staining Experiment. The changes in chromatin organization in HeLa cells after photoirradiation were determined microscopically after treatment with complexes **2**−**4** by dual staining method using acridine orange (AO) and ethidium bromide (EB). Briefly, about 2×10^4 cells were allowed to adhere overnight on a coverslip placed in each well of a 12-well plate. The cells were treated with the complexes **2**−**4** (10 μM) for 4 h in the dark, followed by irradiation with visible light of 400−700 nm (10 J cm^{-2}). Dark controls were also used. The cells were allowed to recover for 1 h, washed thrice with DPBS, stained with an AO/EB mixture (1:1, 10 μM) for 15 min, and observed with a confocal laser scanning microscope (Zeiss LSM 510 apochromat).

Propidium Iodide Staining. The changes in chromatin organization after photoirradiation in HeLa cells were also determined after treatment with complexes **2**−**4** by propidium iodide staining. Similar to the former procedure, about 2×10^4 cells were allowed to adhere overnight on a coverslip placed in each well of a 12-well plate. The cells were treated with the complexes (10 μM) for 4 h in the dark, followed by irradiation with visible light of 400−700 nm (10 J cm^{-2}). Dark controls were also used. The cells were fixed and permeabilized using chilled methanol and kept for 10 min. They were treated with PI (1.0 mg mL^{-1} in DPBS), and images were recorded with a fluorescence microscope (Olympus IX 81). The apoptotic cells were identified by the presence of highly condensed nuclei as opposed to the untreated cells or cells treated with the complexes but unexposed to light, which showed intact cellular morphology.

DNA Binding Methods. Viscometric titrations were performed with a Schott AVS 310 Automated Viscometer at 37 °C. The initial concentration of ct-DNA was 150 μM in NP (nucleotide pair), and the flow times were measured with an automated timer. Data were presented as $(\eta/\eta_0)^{1/3}$ versus [complex]/[DNA], where η is the viscosity of DNA in the presence of the complex and η_0 is that of ct-DNA alone. Viscosity values were calculated from the observed flow time of DNA-containing solutions (t) corrected for that of the buffer alone (t_0), $\eta = (t - t_0)/t_0$.

DNA melting experiments were carried out by monitoring the absorption intensity of ct-DNA (200 μM) at 260 nm at various temperatures, both in the absence and presence of the complexes (20 μM) using a Perkin-Elmer 650 spectrophotometer with a temperature controller. The absorption band at 260 nm of ct-DNA was measured as a function of increasing the temperature in the presence and absence of the iron(III) complexes (20 μM) in phosphate buffer comprising 5 mM Na_2HPO_4, 5 mM NaH_2PO_4, 1 mM Na_2EDTA, and 5 mM NaCl (pH = 6.8).

The experiments were carried out in Tris-HCl buffer (5 mM, pH = 7.2) using solutions of the complexes **1**−**4** in DMF. Calf thymus DNA (ct-DNA, ca. 250 μM) in the buffer medium gave a ratio of UV absorbance at 260 and 280 nm of ca. 1.9:1, suggesting the DNA was apparently free from protein. The concentration of DNA was estimated from its absorption intensity at 260 nm with ε value of 6600 M^{-1} cm^{-1}.[46] Absorption titration experiments were performed by varying the concentration of ct-DNA while keeping the complex concentration as constant. Due correction was made for the absorbance of ct-DNA itself. The spectra were recorded after equilibration for 5 min. The intrinsic equilibrium binding constant (K_b) of the complexes to ct-DNA were obtained by the McGhee−von Hippel (MvH) method using the expression of Bard and co-workers by monitoring the change of the absorption intensity of the spectral

dx.doi.org/10.1021/ic4028173 | Inorg. Chem. 2014, 53, 2152−2162

Table 1. Selected Physicochemical Data for Complexes 1−4

complex	λ (nm) (ε/M^{-1} cm^{1})[a]	IR (O−H)[b] (cm^{-1})	Λ_M[c] (S m^2 M^{-1})	E_{pc}[d] (V)	μ_{eff}[e]	K_b[f] (M^{-1})	ΔT_m[g] (°C)
1	560 (720)	3320	69	−0.56	5.83	(6.4 ± 1.1) × 10^4	1.2
2	505 (1240)	3350	72	−0.58	5.85	(1.0 ± 0.6) × 10^5	3.5
3	490 (1400)	3360	71	−0.59	5.83	(2.5 ± 0.7) × 10^5	4.1
4	434 (3890)		70	−0.59	5.86	(9.3 ± 0.9) × 10^4	3.2

[a]In 6% DMF/Tris-HCl buffer (pH 7.2), as shoulder. [b]In solid phase. [c]Molar conductivity values in DMF at 25 °C. [d]Cathodic peak potential of the Fe(III)/Fe(II) couple vs SCE in MeCN/0.1 M TBAP at a scan rate of 50 mV s^{-1}. [e]Effective magnetic moment of solid samples at 25 °C. [f]Intrinsic calf thymus DNA binding constant. [g]Change in the calf thymus DNA melting temperature in phosphate buffer (pH = 6.8).

bands with increasing concentration of ct-DNA by regression analysis using the equation $(\varepsilon_a - \varepsilon_f)/(\varepsilon_b - \varepsilon_f) = (b - (b^2 - 2K_b^2C_t[DNA]_t/s)^{1/2})/2K_b$, $b = 1 + K_bC_t + K_b[DNA]_t/2s$, where ε_f is the extinction coefficient of free metal complex, ε_a is the extinction coefficient of the complex at a given DNA concentration, ε_b is the extinction coefficient of the absorption peak arising when the complex fully bound to DNA, C_t is the total complex concentration, $[DNA]_t$ is the concentration of DNA, and s is the MvH equation-fitting parameter.[47,48] The nonlinear least-squares analysis was done using Origin Lab, version 8.

DNA Cleavage Experiments. Photoinduced cleavage of supercoiled (SC) pUC19 DNA by complexes **1**−**4** was studied in red light of 647 nm and in green light of 532 nm wavelength, using a continuous-wave (CW) argon−krypton mixed gas ion laser (50 mW laser power, Spectra Physics model Stabilite 2018-RM). The experiments were performed in a total volume of 20 μL containing SC DNA (1 μL, 30 μM) and the complex (20 μM) in a 50 mM Tris HCl buffer (pH = 7.2) containing 50 mM NaCl. The samples were irradiated, after which they were incubated for a further period of 1 h at 37 °C in dark, followed by addition of the loading dye (25% bromophenol blue, 0.25% xylene cyanol, and 30% glycerol (2 μL)), and finally loaded on a 1% agarose gel containing 1 μg mL^{-1} of ethidium bromide (EB). The gels were run at 50 V for 2 h in Tris−acetate−EDTA buffer. The bands were visualized in UV light and photographed, and the intensities of the bands were quantified using the UVITECH Gel Documentation System. Due corrections were made for the trace amount of nicked circular (NC) form present in the original SC DNA and the higher affinity of EB for binding to NC and to linear forms of DNA over the SC form.[49] The error in measuring the band intensities varied from 3 to 5%. Mechanistic studies were done using different additives (DMSO, 4 μL; KI, 0.5 mM; TEMP, 0.5 mM; DABCO, 0.5 mM; NaN_3, 0.5 mM; and catalase, 4 units) that were added to SC DNA prior to the addition of the complex. After light exposure, each sample was incubated for 30 min at 37 °C and analyzed for the photocleaved products using gel electrophoresis.

Theoretical Studies. The geometry of complex **3** was optimized by density functional theory (DFT) method using B3LYP/LanLD2Z level as implemented in Gaussian 09 program. The electronic transitions with their transition probability were obtained using linear response time dependent density functional theory (TDDFT).

RESULTS AND DISCUSSION

Synthesis and General Aspects. The ligands *N,N*-bis(2-pyridylmethyl)-2-aminoethyl-β-D-glucopyranoside (bpyag) and 3-(2-hydroxyphenylimino)-1-phenylbutan-1-one (H_2phap) were synthesized by reported methods.[37] Ligands H_2anap and H_2pyap were synthesized in good yields by a general three-step procedure in which anthracene or pyrene was initially acetylated, followed by a Claisen condensation reaction with ethyl acetate in presence of sodium sand. Finally, the ligands were obtained from Schiff base reaction with 2-aminophenol (Figure S1, Supporting Information). The ligands were characterized from ^{1}H NMR spectral data (Figures S2−S4, Supporting Information). Complexes **1**−**4** were synthesized in good yields from the reaction of $Fe(NO_3)_3{\cdot}9H_2O$ with the tridentate carbohydrate (for **1**−**3**) or phenyl dipicolylamine (for **4**) derivative and the other tridentate ligand in the presence of triethylamine in methanol (Chart 1). The carbohydrate moiety was appended to the ligands to enhance the cellular uptake and solubility of the complex. Complexes **1**−**3** showed better aqueous solubility than the control species **4**, which lacks the carbohydrate moiety. The ligands were chosen to have a phenolic oxygen to enhance the stability of the iron(III) complex and to have a low-energy ligand-to-metal charge transfer (LMCT) band from phenolate π orbital to the dπ* orbital of iron(III). This LMCT band enabled us to study the red light-induced DNA cleavage activity and cytotoxicity of the complexes. We have recently reported an iron(III) catecholate complex showing red light-induced photocytotoxicity and nuclear uptake in HeLa cells.[34] However, the disadvantage associated with this catecholate complex is the presence of a metal-bound nitrate anion, which is found to be labile, resulting in the formation of an aqua adduct in the buffer medium. The presence of a labile site for iron(III) complex is undesirable, considering the high binding affinity of transferrin to iron(III), making the complex ineffective due to leaching of the metal.[50,51] In the present work, we have tried to circumvent this problem by incorporating two different tridentate ligands in the ternary 6-coordinate structure, ensuring higher stability of the complex in the cellular medium. The pendant anthracene or pyrene unit is used to introduce planarity to the molecules that may assist in binding to ct-DNA. As mentioned above, the carbohydrate moiety is attached to enhance the solubility and cellular uptake of the complexes. The phenyl analogue **1** was synthesized and used as a control complex.

Complexes **1**−**4** were characterized from the analytical and physicochemical data (Table 1). The ESI-MS of the complexes **1**−**4** in methanol showed primarily the complex cationic peak $[M - NO_3^-]^+$, suggesting the stability of the complexes under experimental conditions (Figures S5−S8, Supporting Information). The complexes displayed a low-energy phenolic π to iron(III) dπ* orbital LMCT band that extends up to the PDT spectral window of 600−800 nm (Figure 1). The bands for **2** and **3** were largely masked by the high-intensity ligand-centered bands and appeared as an indistinct shoulder in the absorption spectrum. The bands in the UV region correspond to the π−π* transitions of the aromatic anthracene and pyrene moieties. The IR spectra of the complexes **1**−**3** displayed a characteristic broad band near 3000 cm^{-1}, corresponding to the O−H stretching from the carbohydrate moiety, and the band for the nitrate anion at ∼1370 cm^{-1} (Figure S9, Supporting Information). The complexes are 1:1 electrolytic, giving a molar conductivity value of ∼70 S m^{-1} M^{-1} in DMF. The cyclic voltammetry measurements, performed in acetonitrile with 0.1 M TBAP, showed an irreversible redox response corresponding to the Fe(III)/Fe(II) couple near −0.60 V versus SCE (Table 1, Figure S10, Supporting Information). The high negative value indicates the stability of the Fe(III) over the Fe(II) state. The irreversible redox responses observed near −1.8 and 1.0 V

dx.doi.org/10.1021/ic4028173 | Inorg. Chem. 2014, 53, 2152−2162

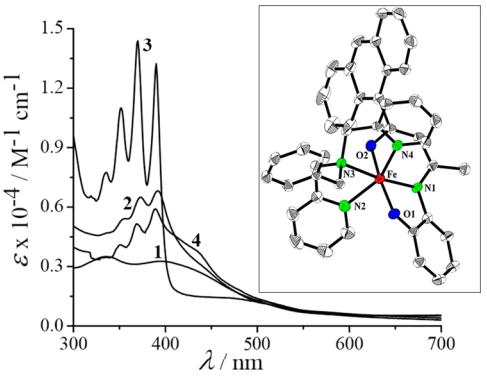

Figure 1. The UV−vis spectra of complexes **1**−**4** in 5% DMF−Tris/HCl buffer (pH = 7.2). The inset shows an ORTEP view of the cationic complex [Fe(dpma)(anap)](PF_6) (**4a**) with thermal ellipsoids at 30% probability level and atom labeling for hetero atoms. The hydrogen atoms are omitted for clarity.

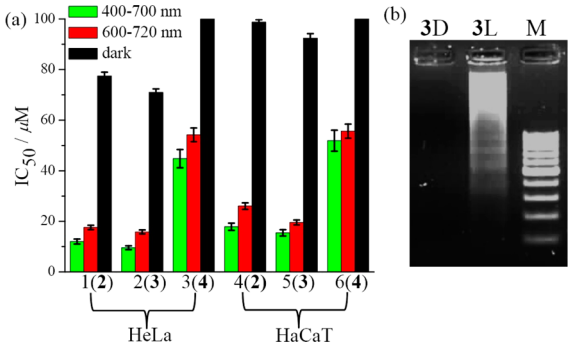

Figure 2. (a) Photocytotoxicity of the complexes **2**−**4** after 2 h incubation followed by irradiation with visible light of 400−700 nm (10 J cm^{-2}, green), red light of 600−720 nm (150 J cm^{-2}, red), and in dark (black) in HeLa (bars 1−3) and HaCaT (bars 4−6) cells, with the complex numbers in parentheses. Bar 1, HeLa and **2**; bar 2, HeLa and **3**; bar 3, HeLa and **4**; bar 4, HaCaT and **2**; bar 5, HaCaT and **3**; bar 6, HaCaT and **4**. (b) DNA ladder of complex **3** upon irradiation in HeLa cells indicating apoptotic cell death (D = dark, L = light, M = Marker 100 bp).

were due to the Schiff base phenolate ligands. The carbohydrate ligand did not show any redox response within the experimental potential window (Figure S11, Supporting Information). The complexes have a high-spin Fe(III) center, giving a magnetic moment value of ∼5.9 μ_B at 25 °C.

X-ray Crystal Structure. Complex **4** was crystallized from a 1:1 (v/v) solution of acetonitrile and methanol as a hexafluorophosphate salt (**4a**.MeCN) and characterized by X-ray crystallography. The ORTEP diagram is shown as inset of Figure 1 (unit cell packing diagram in Figure S12, Supporting Information). Crystallographic parameters are given in Table S1, Supporting Information, and selected bond lengths and bond angles are given in Table S2, Supporting Information. The crystals belong to the $P2_1/a$ space group of the monoclinic system. The molecular structure of the complex has a distorted octahedral N_4O_2 coordination around iron, in which the N,N,N-donor phenyldipicolylamine and the anthracene-appended Schiff base bind to the metal in a facial manner. The Schiff base binds to iron through the enolate and phenolate oxygen atoms and a nitrogen atom, thus showing the tridentate O,N,O-donor mode of bonding. The Fe(1)−O(1) and Fe(1)−O(2) bond distances are 1.899(3) and 1.960(3) Å, respectively. The enolate oxygen is involved in conjugation with the adjacent double bond, and hence the bond is longer compared to the phenolate bond. The Fe−N distances range within 2.0−2.2 Å. The anthracene moiety in the pendant mode does not show any steric encumbrance.

Solubility and Stability. The complexes were soluble in methanol, ethanol, acetonitrile, dimethylformamide, and dimethyl sulfoxide, while being insoluble in hydrocarbon solvents. Complexes **1**−**3**, having the carbohydrate moiety, were partially soluble in water. The stability of the complexes was measured from the time-dependent UV−vis spectral scans. They were found to be stable in aqueous DMF or DMSO, as seen from the spectra acquired after different time intervals and suitable for cellular studies in an aqueous medium (Figure S13, Supporting Information).

Cytotoxicity. The photocytotoxicity of the complexes **1**−**4** along with the ligands were examined in human cervical cancer cell line (HeLa) and human keratinocyte (HaCaT) cells (Figure 2, Figures S14, S15, Supporting Information). The complexes were incubated for 4 h and then irradiated with either visible light of 400−700 nm (10 J cm^{-2}) or red light of 600−720 nm (150 J cm^{-2}). Dark controls were used to measure the PDT effect. Complex **1** did not show any significant photocytotoxicity in visible light. Complexes **2**−**4** were remarkably photocytotoxic to both the cells. The IC_{50} values were ∼10 μM for these complexes in visible light of 400−700 nm in HeLa. The IC_{50} values in red light were near 20 μM. The dark toxicity of all the complexes were low with high IC_{50} values (>80 μM). The carbohydrate conjugates did not exhibit any substantial enhancement in the cytotoxicity compared to the phenyl dipicolylamine iron(III) analogue **4** (Table S3, Supporting Information). We envisaged that, due to glucose being present in the media used for the experiments, the carbohydrate-appended complexes were not preferentially internalized by the cancer cells. Thus we explored the photocytotoxicity of the complexes in these cell lines using glucose-free medium, and the incubation time was varied with 2 and 4 h. The modification in the experimental procedure led us to the expected results. The carbohydrate-appended complexes **2** and **3** were seen to be significantly more photocytotoxic in visible light compared to the nonsugar analogue **4** in HeLa cells (Table 2, Figures S14 and S15, Supporting Information). Within 2 h of incubation, complexes **2** and **3** displayed 2- to 3-fold higher photocytotoxicity compared to the control complex **4**. The difference in photocytotoxicity in the cells was more pronounced when incubation time was 2 h than 4 h. Again this effect was more prominent in HeLa cells compared to immortalized HaCaT cells. This could be due to the fact that initially the complexes are ingested via a receptor-mediated pathway in HeLa cells, resulting in differential uptake as observed.[15] However, with the lapse of time the complexes were internalized by diffusion making all of them as taken up indiscriminately. The iron-uptake experiment was performed to further substantiate our observation.

Cellular Iron Content. The photocytotoxicity of complexes **2** and **3** being higher compared to that of **4** for an incubation time of 2 h could be due to differential uptake of the complexes in the cancer cells. To ascertain the fact, the iron content inside HeLa or HaCaT cells was measured by the inductively coupled plasma optical emission spectroscopy (ICPOES) method after incubating the cells with complexes **1**−**4** for 2 and 4 h in dark (Table 3). It was seen that, for **1**−**3**, the order of iron uptake followed the cytotoxicity trend of **3** > **2** > **1**. The iron uptake by

dx.doi.org/10.1021/ic4028173 | Inorg. Chem. 2014, 53, 2152−2162

Table 2. A Comparison of the IC_{50} Values of Selected Compounds in HeLa and HaCaT Cells

	HeLa			HaCaT		
compound	IC_{50} (μM) (visible light)[a]	IC_{50} (μM) (red light)[b]	IC_{50} (μM) (dark)	IC_{50} (μM) (visible light)[a]	IC_{50} (μM) (red light)[b]	IC_{50} (μM) (dark)
1	78.2 ± 1.2	95.0 ± 0.7	>100	87.3 ± 0.7	>100	>100
2	11.0 ± 0.8	16.6 ± 1.1	85.4 ± 1.1	17.3 ± 0.9	29.5 ± 1.1	>100
3	8.2 ± 0.6	17.7 ± 1.0	87.4 ± 1.2	14.5 ± 1.3	26.2 ± 1.0	>100
4	40.3 ± 1.2	54.2 ± 1.1	>100	47.8 ± 1.1	55.7 ± 1.3	>100
Photofrin[c,d]		4.3 ± 0.2	>41			

[a]Cytotoxicity values correspond to 2 h incubation followed by irradiation in visible light of 400−700 nm (10 J cm^{-2}). [b]Cytotoxicity values correspond to 2 h incubation followed by irradiation in red light of 600−720 nm (150 J cm^{-2}). [c]The values are taken from reference 30 and converted to μM using the approximate molecular weight of Photofrin as 600 g M^{-1}. [d]At 633 nm excitation with fluence rate of 5 J cm^{-2}.

Table 3. Cellular Uptake of Iron (ng/mg Protein) in HeLa and HaCaT Cells for Incubation with 10 μM of the Complexes 1−4 for 2 and 4 h

sample	HeLa		HaCaT	
	2 h	4 h	2 h	4 h
cells alone		0.1		0.2
1	3.9	4.7	1.4	4.4
2	4.0	5.2	2.3	4.9
3	4.9	6.1	2.5	5.1
4	1.1	3.9	1.3	3.6

the cells treated with **4** for 2 h incubation was about four to five times lower than its carbohydrate analogue in HeLa cells. The effect was somewhat less prominent in HaCaT cells. However, cells incubated with **1**−**4** for 4 h showed similar iron content. Thus the difference in photocytotoxicity observed can be explained on the preferential internalization of the carbohydrate-appended complexes in cancer cells in 2 h by receptor-mediated endocytosis. With the lapse of time the difference in amount of the complex ingestion decreases in the cells, giving similar photocytotoxicity of **2**−**4**, possibly due to cellular uptake by diffusion mechanism.[15]

DNA Fragmentation Analysis by Agarose Gel Electrophoresis. Apoptotic DNA fragmentation indicates programmed cell death. Apoptosis is due to the activation of endogenous endonucleases, leading to cleavage of chromatin DNA into internucleosomal fragments of about 180 base pairs (bp) and its multiples thereof. Apoptotic DNA fragmentation could be analyzed using agarose gel electrophoresis, which appears as a ladder-like pattern at 180 bp intervals. Necrosis on the other hand is usually characterized by random DNA fragmentation that forms a "smear" on agarose gels. Complexes **2** and **3** were tested to ascertain the mode of cell death, using the fragmentation of genomic DNA. DNA ladder was observed in HeLa and HaCaT cells on treatment with both the complexes (10 μM) and on irradiation in visible light of 400−700 nm (10 J cm^{-2}) (Figure 2 and Figure S16, Supporting Information). However, no such DNA ladder was evidenced when the cells were treated with the complexes in dark, indicating a photoinduced cell death via an apoptotic pathway.

DCFDA Assay for Measuring Generation of ROS. We have used DCFDA to detect cellular ROS.[46] Cell-permeable DCFDA on oxidation by cellular ROS generates the fluorescent product DCF, with an emission band of 529 nm. The percentage of cell population generating ROS can be determined by flow cytometry analysis. In our experiments we recorded fluorescence of cells alone and those treated with DCFDA alone or DCFDA and complexes **2**−**4** after irradiation with visible light of 400−700 nm for 30 min or incubated in dark for 30 min for controls. The substantial shift in the fluorescence bands observed for cells treated with the complexes compared to the cells treated with the dye alone or the dark controls indicated the generation of ROS (Figure 3(a), Figures S17 and S18, Supporting Information).

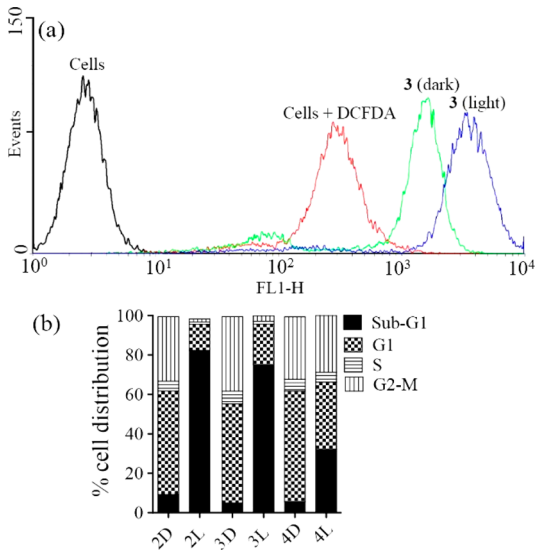

Figure 3. (a) FACS for ROS generation by complex **3** using DCFDA dye. Generation of ROS is highlighted by the shift in fluorescence band positions compared to cells alone in HeLa cells treated with complex **3**, under different experimental conditions as shown by the color codes. Greater shift implies higher amount of DCF and thus greater ROS generation. (b) Bar diagram showing cell cycle distribution (sub-G1, G1, S, and G2/M phases) of the HeLa cells treated with complexes **2** and **4** (10 μM) and irradiated with visible light of 400−700 nm (10 J cm^{-2}), along with the dark controls.

FACS Analysis. To examine the role of the complexes in the cell cycle, the DNA content of the cells treated with complexes **2** and **4** was measured using a fluorescent dye, namely, propidium iodide (PI) in a flow cytometer (Figure 3(b), Figure S19, Supporting Information). The experiments were performed under both light and dark conditions. The complexes in dark did not induce any significant change (<10%) in the sub-G1 population (which indicates cell death) of the cells. Complex **4** on irradiation stimulated modest cell death (~29%). However, under identical experimental conditions, complex **2** showed a marked difference in the population of sub-G1 phase (~82%). These figures are in accord with the trend of cellular uptake. Because of preferential ingestion of complex **2** in HeLa cells, the percentage of cell death is nearly 2.5 times higher than that of complex **4**. The

dx.doi.org/10.1021/ic4028173 | Inorg. Chem. 2014, 53, 2152−2162

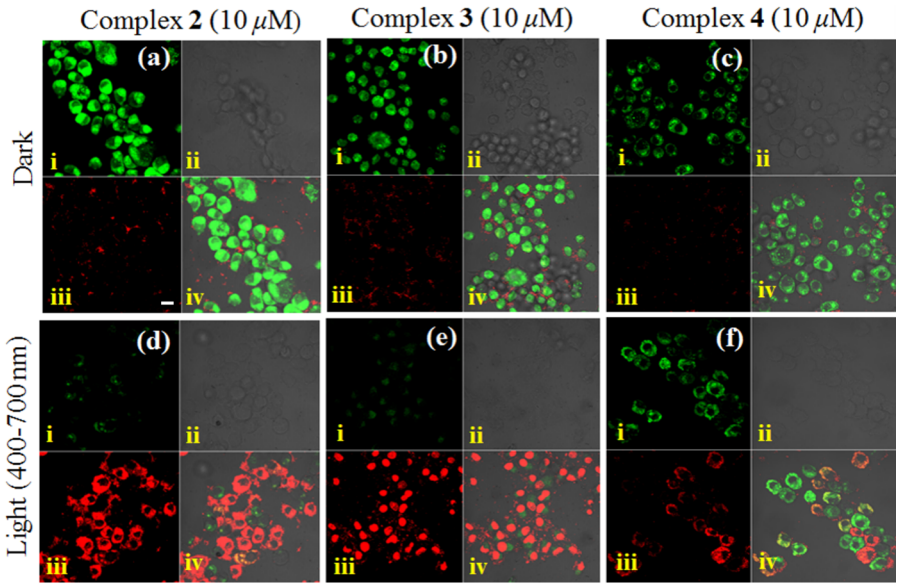

Figure 4. Confocal microscopy images of HeLa cells treated with complexes **2** (a, d), **3** (b, e), and **4** (c, f) on (a–c) keeping in dark or (d–f) irradiated with visible light (400–700 nm, 10 J cm^{-2}) after staining with EB/AO (1:1, 10 μM) solution. (i) Fluorescence of AO. (ii) Bright field images of the cells. (iii) Fluorescence of EB. (iv) The merged images of the former panels. Scale bar in panel (a)-iii is 8.5 μm.

cellular data establish the fact that the carbohydrate-appended complexes are internalized inside the cancer cells at a faster rate, compared to the control.

Ethidium Bromide/Acridine Orange Dual Staining. An EB/AO dual staining experiment was performed in HeLa cells with the complexes **2**–**4** to further investigate their differential uptake property and ability to induce cell death. The experiment was based on the discrimination of live cells from the dead cells on the basis of membrane integrity. AO, which can pass through the plasma membrane, stains the DNA of live cells and fluoresces green. EB on the other hand is excluded from the cells having intact plasma membrane and stains the DNA of dead cells, showing orange fluorescence. The cells incubated with the complexes **2** and **3** for 2 h and irradiated with visible light (400–700 nm, 10 J cm^{-2}) showed significant reddish-orange emission characteristic of the apoptotic cells (Figure 4). The controls, which were incubated in dark, showed only prominent green emission. Complex **4** behaved rather differently than its carbohydrate analogues. Cells treated with **4** under identical experimental conditions did not show any significant orange emission, thus excluding the possibility of cell death. This further confirms the differential uptake of the carbohydrate-appended complexes and their noncarbohydrate analogue.

Propidium Iodide Staining. A PI staining experiment was performed to study the change in cell morphology in HeLa cells upon treating with the complexes **2**–**4** before and after irradiation with visible light (400–700 nm, 10 J cm^{-2}). Significant changes in nuclear morphology, such as chromatin condensation and cell shrinkage, was observed in the cells treated with complex **2** or **3** as compared to the evenly stained nuclear contours of untreated HeLa cells (Figure S20, Supporting Information). Complex **4** did not induce any such chromatin condensation. The results indicate that complexes **2** and **3** are preferentially taken up in the cells by a receptor-mediated pathway, which is not the case for **4**.

DNA Binding. Interaction of the complexes **1**–**4** with ct-DNA was studied by several methods, specifically, viscosity, DNA melting measurements, and UV–vis absorption. Viscosity titrations were conducted using DMF solutions of the complexes and ct-DNA at 37 °C. EB and Hoechst dye were used as references as typical DNA intercalator and groove binder, respectively. From the plot of $(\eta/\eta_0)^{1/3}$ versus [complex]/[DNA], it appears that complexes **2**–**4** bind to DNA via partial intercalation mode (Figure S21, Supporting Information). Complex **1** showed primarily groove binding propensity to ct-DNA. The DNA melting experiments done in phosphate buffer (pH = 6.8) to examine the thermal stability of ct-DNA upon binding to the complexes gave a melting temperature (T_m) increased by a maximum of 4.1 °C for **3**, and the value of ΔT_m ranged within 1–4 °C for the other complexes (Figure S21, Supporting Information). The complexes having a pyrenyl or anthracenyl moiety upon binding to DNA stabilize the double helix and hence require higher temperature for the strands to break. The equilibrium binding constants (K_b) were measured from UV–vis spectral titration of the complexes with ct-DNA in 5% DMF–Tris buffer (pH = 7.2). The decrease in the absorption of the ligand-centered bands near 380 nm was monitored for the complexes. The K_b values were ~10^5 M^{-1}, giving the order of **3** > **2** > **4** > **1** (Figure S22, Supporting Information). The planarity of the pyrene and anthracene groups makes the complexes better binders to ct-DNA than the phenyl analogue.

DNA Cleavage and Mechanistic Aspects. The chemical nuclease activity of the complexes (20 μM) was studied in the presence of external oxidizing (H_2O_2, 0.5 mM) and reducing (glutathione (GSH), 0.5 mM) agents using supercoiled (SC) pUC19 DNA (30 μM bp, 0.2 μg) in Tris-HCl/NaCl buffer (50 mM, pH 7.2) in dark. The Fe(III) complexes on treating with GSH or H_2O_2 did not show any significant DNA cleavage activity. They also did not show any significant hydrolytic cleavage of DNA (Figure S23, Supporting Information). The undesired hydrolytic cleavage of DNA is thus prevented by blocking all the coordination sites of Fe(III) by appropriately designed ligand systems and, in addition, making the iron(III)

dx.doi.org/10.1021/ic4028173 | Inorg. Chem. 2014, 53, 2152–2162

complexes as chemical-nuclease inactive by stabilizing the iron(III) redox state.

The photoinduced DNA cleavage activity of the complexes **1**−**4** was studied using SC pUC19 DNA (30 μM, 0.2 μg) in a medium of Tris-HCl/NaCl (50 mM, pH 7.2) buffer on irradiation with red light of 647 nm (50 mW) and green light of 532 nm (50 mW) using a CW argon−krypton mixed gas ion laser. The extent of DNA cleavage is shown in the gel electrophoresis diagram (Figure 5). Control experiments using

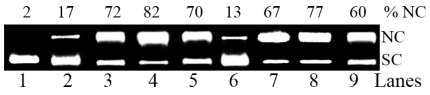

Figure 5. Gel diagram showing the photocleavage of SC pUC19 DNA (0.2 μg, 30 μM) by the complexes **1**−**4** in Tris-HCl buffer (pH 7.2) containing 10% DMF on photoexposure to green light of 532 nm (t = 1 h, lanes 2−5) and red light of 647 nm (t = 2 h, lanes 6−9): lane 1, DNA control; lane 2, DNA and **1** (15 μM); lane 3, DNA and **2** (15 μM); lane 4, DNA and **3** (15 μM); lane 5, DNA and **4** (15 μM); lane 6, DNA and **1** (20 μM); lane 7, DNA and **2** (20 μM); lane 8, DNA and **3** (20 μM); lane 9, DNA and **4** (20 μM).

the metal salt and the phenolate or the carbohydrate ligands in light and the complexes in dark did not show any significant DNA cleavage activity (Figure S24, Supporting Information). Complex **1**, with a pendant phenyl group on the phenolate ligand, showed modest DNA photocleavage activity. Complexes **2**−**4** were, however, highly active, showing significant DNA cleavage activity in both green and red light. Photolysis of SC DNA with a 15 μM solution of **2**−**4** in green light of 532 nm showed ∼80% cleavage of SC DNA on photoexposure for 1 h. Similarly a 20 μM solution of **2** or **4** induced ∼70% cleavage of SC DNA on exposure to red light for 2 h. Complex **3** showed almost 80% cleavage of SC DNA to its nicked circular (NC) form under similar reaction conditions.

Mechanistic investigations were carried out using complexes **2** and **3**. The DNA groove binding propensity of the complexes was studied using the minor groove binder distamycin-A and the major groove binder methyl green. Distamycin-A or methyl green showed ∼10% cleavage of SC DNA in red light of 647 nm. Addition of **2** or **3** to distamycin-A-bound SC DNA did not show any inhibition in the DNA cleavage activity. However, addition of methyl green to **2** or **3** significantly inhibited the DNA photocleavage activity thus suggesting DNA binding of the complexes via DNA major groove. The complexes did not induce any significant photocleavage of DNA in argon medium, indicating the possible involvement of the ROS in the DNA photocleavage reactions. Addition of singlet oxygen quenchers, specifically, DABCO, TEMP, and sodium azide, showed no apparent effect on the DNA cleavage activity, thus ruling out the possibility of a type-II singlet oxygen pathway, which is known for the PDT activity of organic macrocyclic dyes like Photofrin (Figure S25, Supporting Information). In contrast, hydroxyl radical scavengers, specifically, DMSO, KI, and catalase, showed significant inhibition in the DNA photocleavage activity in both the light sources used. The mechanistic data indicate the formation of hydroxide and superoxide radicals as the ROS in a photoredox pathway whereby metal reduction follows the photoactivation of the LMCT band, forming charge-separated Fe^{2+}-$L^{\bullet+}$ (phenolate−ligand radical cation) as the reactive species that possibly reduces O_2 to $O_2^{\bullet-}$ by the reactive Fe^{2+} ion and generates hydroxyl radicals via the reaction $3O_2^{\bullet-} + 2H^+ \rightarrow HO^{\bullet} + HO^- + 2O_2$. Such a mechanism is reported for the iron(III) complexes having phenolate ligands.[52]

Theoretical Study. DFT calculations were carried out using b3LYP/LAN2DZ level with Gaussian 03 programs to get further insights on the excited-state properties. Calculations were performed on the geometrically optimized structure of **3** (Figure S26, Supporting Information). The dipole-allowed transitions for the complex are listed in Table S4, Supporting Information. This structure showed a highly favored transition band with a peak in the visible region at 437 nm having oscillator strength of 0.25. These transitions that were assigned as LMCT bands involving the phenolate to the iron(III) center are likely to be responsible for the generation of ROS, resulting in the photocytotoxicity of the complexes. The high oscillator strength indicates the probability of formation of charge-separated reactive species that possibly reduce O_2 to $O_2^{\bullet-}$, eventually leading to the formation of hydroxyl radical species.[52] Transitions occurring below 400 nm are ligand-based, involving the pyrene group. There are mainly three transitions at 388, 376, and 373 nm having oscillator strengths between 0.02−0.01. From the molecular orbital pictures it is seen that for complex **3**, the HOMO mainly resides on the electron-rich pyrene group while the LUMO has significant contributions from the adjacent aminophenol group (Figure 6). The proximity of the HOMO and LUMO accounts for the absence of any significant fluorescence in the complex, despite having a pyrene group.

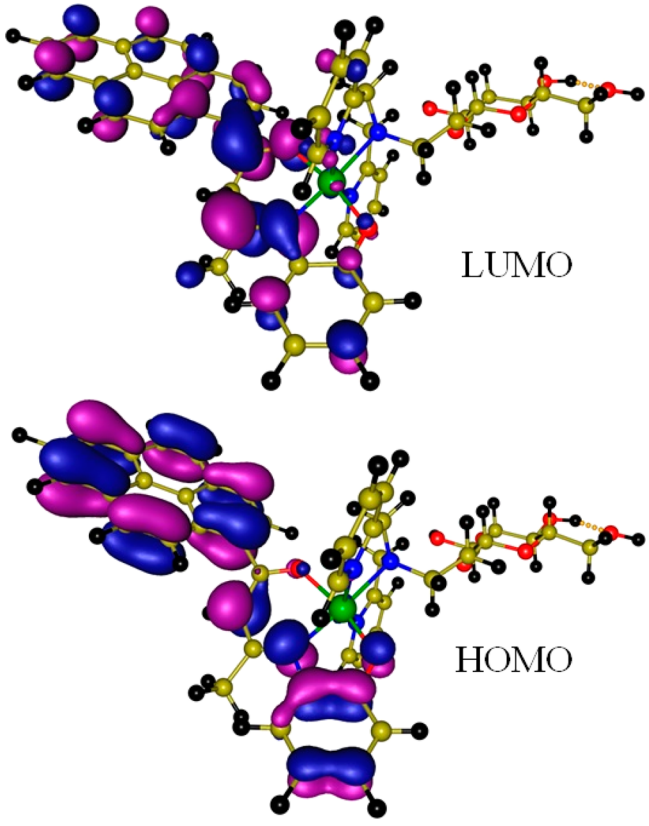

Figure 6. The HOMO and LUMO of complex **3** as obtained from the DFT calculations. The energy of the HOMO is −7.29 eV and that of the LUMO is −4.28 eV.

dx.doi.org/10.1021/ic4028173 | Inorg. Chem. 2014, 53, 2152−2162

CONCLUSIONS

This report presents new ternary iron(III) complexes showing significant photocytotoxicity in red light with low dark toxicity. The carbohydrate-appended complexes were seen to be internalized preferentially in the HeLa cells with respect to the control complex, which lacks the carbohydrate moiety. The complexes having two different tridentate ligands in a six-coordinate structure are stable in the aqueous medium. The observed photocytotoxicity in red light is of importance, considering greater tissue penetration power of low-energy light. The complexes caused cell death in an apoptotic pathway by the generation of ROS on irradiation. The dark toxicity is found to be significantly low due to the structural stability and the absence of any hydrolytic DNA cleavage and chemical nuclease activity. The results are of significance toward developing targeted metal-based PDT agents in red light using iron as the bioessential metal ion.

ASSOCIATED CONTENT

Supporting Information

Tables of crystallographic data, bond lengths, and bond angles for complex **4a**, IC_{50} values of selected compounds in HeLa and HaCaT cells, excited-state transitions in complex **3**, Figures showing structures in synthesis of ligand H_2pyap, NMR spectra of ligands, ESI-MS and IR spectra of complexes, other Figures and data as described in text. This material is available free of charge via the Internet at http://pubs.acs.org.

AUTHOR INFORMATION

Corresponding Author

*E-mail: arc@ipc.iisc.ernet.in. (A.R.C.) Phone: +91-80-22932533. Fax: +91-80-23600683. E-mail: paturu@mrdg.iisc.ernet.in. (P.K.) Phone: +91-80-22933259.

Notes

The authors declare no competing financial interest.

ACKNOWLEDGMENTS

We thank the Department of Science and Technology (DST), Government of India, and the Council of Scientific and Industrial Research (CSIR), New Delhi, for financial support (SR/S5/MBD-02/2007; CSIR/01(2559)/12/EMR-II/2012). A.R.C. thanks the DST for J. C. Bose National Fellowship and the Alexander von Humboldt Foundation, Germany, for donation of an electrochemical system. I.K. and A.H. thank CSIR for research fellowships. We are thankful to Dr. O. Joy, P. Pai, and A. Kavya for the FACS analysis, to Deepti Bapat for the confocal and fluorescence microscopy data, and to K. Mitra for the ESI-MS data. We thank Prof. Sudhakar Rao, Civil Engineering Department of our institute for the ICPOES facility.

REFERENCES

(1) Ethirajan, M.; Chen, Y.; Joshi, P.; Pandey, R. K. *Chem. Soc. Rev.* **2011**, *40*, 340−362.
(2) Bonnett, R. *Chemical Aspects of Photodynamic Therapy;* Gordon & Breach: London, U.K., 2000.
(3) DeRosa, M. C.; Crutchley, R. J. *Coord. Chem. Rev.* **2002**, *233*−*234*, 351−371.
(4) Clichici, S.; Filip, A.; Daicoviciu, D.; Ion, R. M.; Mocan, T.; Tatomir, C.; Rogojan, L.; Olteanu, D.; Muresan, A. *Acta Physiol. Hung.* **2010**, *97*, 41−51.
(5) Fan, N. C.; Cheng, F. Y.; Ho, J. A.; Yeh, C. S. *Angew. Chem., Int. Ed.* **2012**, *51*, 8806−8810.
(6) Macheda, M. L.; Rogers, S.; Best, J. D. *J. Cell. Physiol.* **2005**, *202*, 654−662.
(7) MacIver, N. J.; Jacobs, S. R.; Wieman, H. L.; Wofford, J. A.; Coloff, J. L.; Rathmell, J. C. *J. Leukocyte Biol.* **2008**, *84*, 949−957.
(8) Hanif, M.; Meier, S. M.; Kandioller, W.; Bytzek, A.; Hejl, M.; Hartinger, C. G.; Nazarov, A. A.; Arion, V. B.; Jakupec, M. A.; Dyson, P. J.; Keppler, B. K. *J. Inorg. Biochem.* **2011**, *105*, 224−231.
(9) Hussein, Y. R.; Bandyopadhyay, S.; Semaan, A.; Ahmed, Q.; Albashiti, B.; Jazaerly, T.; Nahleh, Z.; Ali-Fehmi, R. *Clin. Transl. Oncol.* **2011**, *4*, 321−327.
(10) Ballut, S.; Makky, A.; Chauvin, B.; Michel, J. P.; Kasselouri, A.; Maillard, P.; Rosilio, V. *Org. Biomol. Chem.* **2012**, *10*, 4485−4495.
(11) Zheng, X.; Pandey, R. K. *Anti-Cancer Agents Med. Chem.* **2008**, *8*, 241−268.
(12) Zheng, X.; Morgan, J.; Pandey, S. K.; Chen, Y. E.; Baumann, T. H.; Missert, J. R.; Batt, C.; Jackson, J.; Bellnier, D. A.; Henderson, B. W.; Pandey, R. K. *J. Med. Chem.* **2009**, *52*, 4306−4318.
(13) Sakuma, S.; Otake, E.; Torii, K.; Nakamura, M.; Maeda, A.; Tujii, R.; Akashi, H.; Ohi, H.; Yano, S.; Mohita, A. *J. Porphyrins Phthalocyanines* **2013**, *17*, 331−342.
(14) Calvaresi, E. C.; Hergenrother, P. J. *Chem. Sci.* **2013**, *4*, 2319−2333.
(15) Hirohara, S.; Obata, M.; Ogata, S.; Kajiwara, K.; Ohtsuki, C.; Tanihara, M.; Yano, S. *J. Photochem. Photobiol., B* **2006**, *84*, 56−63.
(16) Hirohara, S.; Obata, M.; Ogata, S. I.; Ohtsuki, C.; Higashida, S.; Ogura, S. I.; Okura, I.; Takenaka, M.; Ono, H.; Sugai, Y.; Mikata, Y.; Tanihara, M.; Masao, Y.; Yano, S. *J. Photochem. Photobiol., B* **2005**, *78*, 7−15.
(17) Zorlu, Y.; Dumoulin, F.; Bouchu, D.; Ahsen, V.; Lafont, D. *Tetrahedron Lett.* **2010**, *51*, 6615−6618.
(18) Hocine, O.; Gary-Bobo, M.; Brevet, D.; Maynadier, M.; Raehm, L.; Richeter, S.; Loock, B.; Morère, A.; Maillard, P.; Garcia, M.; Durand, J. O. *Int. J. Pharm.* **2012**, *423*, 509−515.
(19) Shieh, M. J.; Peng, C. L.; Chiang, W. L.; Wang, C. H.; Hsu, C. Y.; Wang, S. J.; Lai, P. S. *Mol. Pharmaceutics* **2010**, *7*, 1244−1253.
(20) Smith, N. A.; Sadler, P. J. *Philos. Trans. R. Soc., A* **2013**, *371*, 20120519 DOI: 10.1098/rsta.2012.0519.
(21) Schatzschneider, U. *Eur. J. Inorg. Chem.* **2010**, 1451−1467.
(22) Chifotides, H. T.; Dunbar, K. R. *Acc. Chem. Res.* **2005**, *38*, 146−156.
(23) Higgins, S. L. H.; Tucker, A. J.; Winkel, B. S. J.; Brewer, K. J. *Chem. Commun.* **2012**, *48*, 67−69.
(24) Fry, N. L.; Mascharak, P. K. *Acc. Chem. Res.* **2011**, *44*, 289−298.
(25) Ford, P. C. *J. Am. Chem. Soc.* **2009**, *131*, 15963−15964.
(26) Ishida, M.; Lim, J. M.; Lee, B. S.; Tani, F.; Sessler, J. L.; Kim, D.; Naruta, Y. *Chem.—Eur. J.* **2012**, *18*, 14329−14341.
(27) Ranyuk, E.; Cauchon, N.; Klarskov, K.; Guérin, B.; van Lier, J. E. *J. Med. Chem.* **2013**, *56*, 1520−1534.
(28) Sgambellone, M. A.; David, A.; Garner, R. N.; Dunbar, K. R.; Turro, C. *J. Am. Chem. Soc.* **2013**, *135*, 11274−11282.
(29) Goswami, T. K.; Chakravarthi, B. V. S. K.; Roy, M.; Karande, A. A.; Chakravarty, A. R. *Inorg. Chem.* **2011**, *50*, 8452−8464.
(30) Saha, S.; Majumdar, R.; Hussain, A.; Dighe, R. R.; Chakravarty, A. R. *Philos. Trans. R. Soc., A* **2013**, *371*, 20120190 DOI: 10.1098/rsta.2012.0190.
(31) Banerjee, S.; Prasad, P.; Hussain, A.; Khan, I.; Kondaiah, P.; Chakravarty, A. R. *Chem. Commun.* **2012**, *48*, 7702−7704.
(32) Sasmal, P. K.; Saha, S.; Majumdar, R.; Dighe, R. R.; Chakravarty, A. R. *Chem. Commun.* **2009**, 1703−1705.
(33) Basu, U.; Khan, I.; Koley, D.; Saha, S.; Kondaiah, P.; Chakravarty, A. R. *J. Inorg. Biochem.* **2012**, *116*, 77−87.
(34) Basu, U.; Khan, I.; Hussain, A.; Kondaiah, P.; Chakravarty, A. R. *Angew. Chem., Int. Ed.* **2012**, *51*, 2658−2661.
(35) Perrin, D. D.; Armarego, W. L. F.; Perrin, D. R. *Purification of Laboratory Chemicals;* Pergamon Press: Oxford, 1980.
(36) Mikata, Y.; Sugai, Y.; Obata, M.; Harada, M.; Yano, S. *Inorg. Chem.* **2006**, *45*, 1543−1551.
(37) Dey, D. K.; Dey, S. P.; Karan, N. K.; Datta, A.; Lycka, A.; Rosair, G. M. *J. Organomet. Chem.* **2009**, *694*, 2434−2441.

(38) Atherton, J. C. C.; Jones, S. *J. Chem. Soc., Perkin Trans. 1* **2002**, 2166−2173.
(39) D'Souza, L. J.; Maitra, U. *J. Org. Chem.* **1996**, *61*, 9494−9502.
(40) Walker, N.; Stuart, D. *Acta Crystallogr., Sect. A* **1983**, *A39*, 158−166.
(41) Sheldrick, G. M. *SHELX-97, Programs for Crystal Structure Solution and Refinement;* University of Göttingen: Göttingen, Germany, 1997.
(42) Johnson, C. K. *ORTEP;* Technical Report ORNL-5138 for Oak Ridge National Laboratory: Oak Ridge, TN, 1976.
(43) Mosmann, T. *J. Immunol. Methods* **1983**, *65*, 55−63.
(44) Keston, A. S.; Brandt, R. *Anal. Biochem.* **1965**, *11*, 1−5.
(45) Takanashi, T.; Ogura, Y.; Taguchi, H.; Hashizoe, M.; Honda, Y. *Invest. Ophthalmol. Visual Sci.* **1997**, *38*, 2721−2728.
(46) Reichman, M. E.; Rice, S. A.; Thomas, C. A.; Doty, P. *J. Am. Chem. Soc.* **1956**, *76*, 3047−3054.
(47) McGhee, J. D.; von Hippel, P. H. *J. Mol. Biol.* **1974**, *86*, 469−489.
(48) Carter, M. T.; Rodriguez, M.; Bard, A. J. *J. Am. Chem. Soc.* **1989**, *111*, 8901−8911.
(49) Bernadou, J.; Pratviel, G.; Bennis, F.; Girardet, M.; Meunier, B. *Biochemistry* **1989**, *28*, 7268−7275.
(50) Brown, P. J.; Molloy, C. M.; Johnson, P. M. *Placenta* **1982**, *3*, 21−27.
(51) Barbeau, K. *Photochem. Photobiol.* **2006**, *82*, 1505−1516.
(52) Maurer, D.; Kraft, B. J.; Lato, S. M.; Ellington, A. D.; Zaleski, J. M. *Chem. Commun.* **2000**, 69−70.

dx.doi.org/10.1021/ic4028173 | *Inorg. Chem.* 2014, 53, 2152−2162